



Combination of the LSMME scheme and causal imaging condition to remove RTM artifacts

Daniel E. Revelo*^{1,2}, Rodrigo S. Santos^{1,2}, Reynam C. Pestana², Marcelo S. Souza^{1,2}, Diego F. Barrera¹, Victor Koehne¹

¹ SENAI/CIMATEC Supercomputing Center, Salvador, Bahia, Brazil

² Federal University of Bahia (UFBA), Salvador, Bahia, Brazil

Copyright 2021, SBGf - Sociedade Brasileira de Geofísica.

This paper was prepared for presentation at the 17th International Congress of the Brazilian Geophysical Society, held in Rio de Janeiro, Brazil, 8 to 11 November, 2021.

Contents of this paper were reviewed by the Technical Committee of the 17th International Congress of the Brazilian Geophysical Society and do not necessarily represent any position of the SBGf, its officers or members. Electronic reproduction or storage of any part of this paper for commercial purposes without the written consent of The Brazilian Geophysical Society is prohibited.

Abstract

Reverse-time migration (RTM) is a wave-equation based imaging technique that is capable of dealing with multipath arrivals and image very steeply dipping reflectors and overhangs. Images produced by the migration of seismic data related to complex geology are often contaminated by artifacts due to the presence of internal multiple reflections. The multiple reflections are interpreted as the main coherent noise in seismic data, and therefore, strategies to remove this noise have been developed, such as the Marchenko multiple elimination (MME) by the least-squares scheme (LSMME). On the other hand, the employed zero-lag imaging condition between the forward-in-time modeled source wavefield and the back-propagated receiver wavefield, aside from constructing the subsurface image, also gives rise to artifacts, generated by the undesired cross-correlation of backscattered waves. A large part of these RTM artifacts can be suppressed by directionally decomposing wavefields before imaging. So, we are proposing a procedure in which the artifacts present in the conventional RTM are mitigated using the LSMME scheme (in the data domain) and applying a causal image condition (in the model domain). To demonstrate the performance of our proposed strategy, we apply it to a 2D numerical example and compare the result with that obtained by the conventional RTM of the original dataset. From the RTM results, we show that the application of both techniques allows the construction of seismic images free of these undesired artifacts.

INTRODUCTION

The use of the seismic reflection method for the study of the interior of the planet is a common practice in the hydrocarbon industry, since with this method it is possible to illuminate regions with kilometers of depth and in high resolution. This study is carried out through the analysis of migrated sections that are constructed using standard seismic migration techniques, such as reverse-time migration (RTM) (Baysal et al., 1983; McMechan, 1983) or Kirchhoff migration. A drawback of these methods is that they rely on the single-scattering assumption, i.e., the recorded seismic data do not include waves that are reflected more than once in the subsurface before reaching

the receivers. These reflections are referred to as internal multiple reflections and are known as the main coherent noise present in the seismic reflection data. The fact that the presence of internal multiple reflections is disregarded during the generation of seismic images through standard imaging methods can lead to the generation of false events in the migrated sections. Therefore, some techniques have been proposed to mitigate the artifacts related to the internal multiples, whose traditional workflow consists of predicting the internal multiples and subtracting them from the acquired seismic data. However, with the recent development of the Marchenko equations, several alternatives have been presented for the treatment of these noises. It is important to mention the work of [van der Neut and Wapenaar \(2016\)](#), where the coupled Marchenko equations are rewritten by projecting the focusing points back to the acquisition surface and presented a scheme to eliminate internal multiple reflections from the measured acoustic wavefield. The main issue with this scheme is that its implementation requires information related to the macro velocity model to create time truncations.

[Zhang and Staring \(2018\)](#) modified the aforementioned scheme and proposed the method called Marchenko multiple elimination (MME), which is a data-driven algorithm. Later, [Zhang et al. \(2019\)](#) used the work of [Zhang and Staring \(2018\)](#) to derive a scheme that eliminates internal multiple reflections and applies compensation for transmission losses contained in primary reflections. These results suggest that the MME scheme may be the best alternative to eliminate internal multiples when the seismic data has previously gone through a high-quality pre-processing stage, i.e., deghosting, removal of free-surface multiples, and deconvolution with an estimated source wavelet. [Zhang and Slob \(2020b\)](#) used a laboratory dataset to evaluate the performance of the MME, obtaining a dataset free of internal multiple reflections. [Zhang and Slob \(2019a\)](#) presented the first example of applying the MME on a field dataset from the Norwegian North Sea, which validated the capabilities of the MME scheme and showed that it can effectively eliminate internal multiples without model information or adaptive subtraction. [Zhang and Slob \(2020a\)](#) developed a fast implementation version that reduces the computational cost of the conventional MME by one order of magnitude. [Santos et al. \(2020b\)](#) took advantage of the fact that the MME scheme is a data-driven algorithm and shown that it is possible to apply it in early seismic processing workflows, allowing to calculate NMO velocity fields by picking the semblance free from the effects of multiples. Recently, [Santos et al. \(2020a\)](#) have proposed to formulate

the application of the MME scheme as a least-squares problem (LSMME) that guarantee the convergence criterion of the Neumann series approximation, which is the proposed solution in the original formulation.

The application of the LSMME scheme allows eliminating the ghost reflectors caused by the internal multiple reflections. Nevertheless, another major drawback of RTM is strong artifacts related to the imaging condition applied to construct the reflectivity image. The conventional imaging condition for RTM is the zero-lag cross-correlation of the source and receiver wavefields. The resulting image obtained by applying the conventional cross-correlation is always contaminated by low-frequency artifacts and false reflectors, which are generated due to the presence of sharp wave-speed contrasts in the velocity model and the undesired cross-correlation of backscattered waves. In recent years, more attention has been given to improve the imaging condition and reduce the low-frequency noise. Different techniques have been proposed in the literature (Baysal et al., 1984; Yoon and Marfurt, 2006; Fletcher et al., 2006; Guitton et al., 2007). A practical approach is to apply the Laplacian filter (Zhang and Sun, 2009), which shows good attenuation of RTM artifacts without hurting steeply dipping reflectors, but it can damage the signal of interest (Guitton et al., 2007).

Another way to address this type of migration artifact is to modify the imaging condition. In this direction, Liu et al. (2011) proposed an imaging condition based on the decomposition of the wavefield into one-way components. The imaging condition introduced by Liu et al. (2011) only allows wave components that propagate in opposite directions to be correlated. This method is an implicit separation that successfully removes many types of artifacts without the need of applying the Laplacian filter. To address the wavefield separation, we usually define the wave-propagation direction in the Fourier domain. In the frequency-wavenumber domain, the wave-propagation is defined by the sign of the frequency and the wavenumber (Hu and McMechan, 1987; Liu et al., 2011). If we use the conventional wavefield decomposition method in the time-domain RTM, we should store the wavefield and perform Fourier transform along the time axis. This process increases the input/output cost because the time axis is the slowest dimension of the stored wavefield and Fourier transform operates most efficiently on data that are stored contiguously. But, if we can define a time-domain wavefield whose spectrum only contains a positive or negative frequency, we can define the wave-propagation direction using the sign of the spatial wavenumber and avoid the I/O cost. This signal is the analytical signal which is a complex signal whose real part is the signal itself and its complex part is the Hilbert transform of the real part. For RTM, we extend the analytic signal concept and call it the analytical wavefield.

In the work of Shen and Albertin (2015) the imaginary part of the analytical wavefield is obtained applying a temporal Hilbert transform to the source term of the wave-equation followed by conventional propagation. The wavefield propagated with conventional source and the wavefield generated by its Hilbert transform, constitute the analytical wavefield. Recently, Revelo and Pestana (2019) proposed an alternative method based

on the first-order partial equation in time and by just solving the wave equation once. This strategy improves the computation of wavefield separation. Because the analytical wavefield only contains positive frequencies, the down- and up-going wave components can then be conveniently obtained by applying 1D Fourier filters in depth. Shen and Albertin (2015) propose a causal imaging condition that correlates the down-going source component with the up-going receiver component for subsurface imaging, which successfully removed many types of RTM artifacts presented in the images obtained from conventional cross-correlation imaging condition.

Based on the fact that conventional RTM image contains artifacts caused by multiple internal reflections and the imaging condition applied to generate the migration section. In this paper, we combined the LSMME scheme and the causal RTM, to attenuate multiple internal reflections and generate a seismic image of high quality and artifacts-free due to backscattered energy, respectively. A numerical example is given to demonstrate the validity of the proposed procedure and the effectiveness of the causal imaging condition in RTM images using as input the retrieved dataset by LSMME scheme. Finally, some conclusions are drawn.

THEORY

The LSMME scheme

We present a brief review of the LSMME scheme proposed in Santos et al. (2020a). For the notation in this work, the spatial coordinates are defined by their horizontal and depth components, for instance, $\mathbf{x}_i = (\mathbf{x}_H, z_i)$, where \mathbf{x}_H are the horizontal coordinates and z_i is the depth of an arbitrary boundary $\partial\mathbf{D}_i$, such that the surface acquisition $\partial\mathbf{D}_0$ will be defined by $\mathbf{x}_0 = (\mathbf{x}_H, z_0)$. The acoustic impulse reflection response from a source at \mathbf{x}_0 (recorded by a pressure receiver at \mathbf{x}'_0) is denoted as $R(\mathbf{x}'_0, \mathbf{x}_0, t)$, where t is the propagation time. The reflection response is represent by $\bar{R}(\mathbf{x}'_0, \mathbf{x}_0, t)$. In practice, R is obtained from deconvolution of \bar{R} with the source time signature. The projected version of the revised Marchenko equations, for the single-sided reflection response, is given by the following expressions in operator form (Zhang and Staring, 2018)

$$\begin{cases} v_m^+(\mathbf{x}'_0, \mathbf{x}_0, t) = (\Theta_\varepsilon^{t_2-\varepsilon} \mathbf{R}^* v^-)(\mathbf{x}'_0, \mathbf{x}_0, t), \\ v^-(\mathbf{x}'_0, \mathbf{x}_0, t) = (\Theta_\varepsilon^{t_2-\varepsilon} \mathbf{R} \delta + \Theta_\varepsilon^{t_2-\varepsilon} \mathbf{R} v_m^+)(\mathbf{x}'_0, \mathbf{x}_0, t), \end{cases} \quad (1)$$

$$U^-(\mathbf{x}'_0, \mathbf{x}_0, t) = (\Theta_{t_2-\varepsilon}^\infty \mathbf{R} \delta + \Theta_{t_2-\varepsilon}^\infty \mathbf{R} v_m^+)(\mathbf{x}'_0, \mathbf{x}_0, t), \quad (2)$$

where U^- is the projected version of the upgoing component of the Green function, and v_m^+ and v^- are named as the down and upgoing filter functions, respectively. The truncation operator $\Theta_\varepsilon^{t_2-\varepsilon}$ excludes values outside of the window $(\varepsilon, t_2 - \varepsilon)$, where ε is a positive value to account for the finite bandwidth and t_2 is the two-way travelttime of the acquisition surface $\partial\mathbf{D}_0$ and a fictitious reflector at horizon $\partial\mathbf{D}_i$. The multidimensional convolution and correlation integral operators, applied on an arbitrary wavefield $P(\mathbf{x}, \mathbf{x}'', t)$, are defined as

$$\{\mathbf{R}P\}(\mathbf{x}'', \mathbf{x}', t) = \int_{\partial\mathbf{D}} d\mathbf{x} \int_{-\infty}^{+\infty} R(\mathbf{x}', \mathbf{x}, t') P(\mathbf{x}, \mathbf{x}'', t-t') dt', \quad (3)$$

$$\{\mathbf{R}^*P\}(\mathbf{x}'', \mathbf{x}', t) = \int_{\partial\mathbf{D}} d\mathbf{x} \int_{-\infty}^{+\infty} R(\mathbf{x}', \mathbf{x}, -t') P(\mathbf{x}, \mathbf{x}'', t-t') dt'. \quad (4)$$

As explained in [Zhang and Staring \(2018\)](#) and [Zhang and Slob \(2019b\)](#), Eq. 2 allows the evaluation of $U^-(\mathbf{x}_0'', \mathbf{x}_0', t)$ for each time instant t_2 . Then, if $U^-(\mathbf{x}_0'', \mathbf{x}_0', t_2)$ is convolved with the source wavelet, its value at t_2 can be collected to be stored in a new function \bar{R}_t , which will contain only primary reflections

$$\bar{R}_t(\mathbf{x}_0'', \mathbf{x}_0', t = t_2) = \bar{U}^-(\mathbf{x}_0'', \mathbf{x}_0', t_2), \quad (5)$$

where the overbar indicates quantities that have been convolved with the source wavelet. The process could be applied for time instant t_2 in the interval $0 \leq t_2 \leq t_{\max}$ (where t_{\max} represents the maximum time recorded in the data set), and the function \bar{R}_t will store all primary reflections free of multiples. The solution of Eq. 1 based on Neumann series approximation is known as the conventional MME scheme ([Zhang et al., 2019](#)). The resulting internal multiple-free reflection response can serve as input for further processing, such as RTM technique.

The computation of \bar{U}^- demands first obtaining v_m^+ . [Santos et al. \(2020a\)](#) have shown that v_m^+ can be obtained if Eq. 1 is formulated as an inverse problem, which can be solved using the least-squares scheme (LS). Then, taking into account that $\{\mathbf{R}\mathcal{D}\}(\mathbf{x}_0'', \mathbf{x}_0', t) = R(\mathbf{x}_0'', \mathbf{x}_0', t)$ ([van der Neut and Wapenaar, 2016](#)), Eq. 1 can be rewritten in the following matrix form

$$\begin{bmatrix} \mathbf{v}^- \\ \mathbf{v}_m^+ \end{bmatrix} = \begin{bmatrix} \Theta R + \Theta \mathbf{R} \mathbf{v}_m^+ \\ \Theta \mathbf{R}^* \mathbf{v}^- \end{bmatrix}, \quad (6)$$

and after some algebraic manipulations, we formulate Eq. 6 as a linear system in the form $\mathbf{A}\mathbf{x} = \mathbf{y}$

$$\underbrace{\begin{bmatrix} \mathbf{I} & -\Theta \mathbf{R} \\ -\Theta \mathbf{R}^* & \mathbf{I} \end{bmatrix}}_{\mathbf{A}} \underbrace{\begin{bmatrix} \mathbf{v}^- \\ \mathbf{v}_m^+ \end{bmatrix}}_{\mathbf{x}} = \underbrace{\begin{bmatrix} \Theta \mathbf{R} \\ \mathbf{0} \end{bmatrix}}_{\mathbf{y}}. \quad (7)$$

Solving Eq. 7 allows us to obtain v_m^+ , which is substituted into Eq. 2 to compute U^- . To solve the linear system (Eq. 7) we have applied an iterative damped least-squares method ([Paige and Saunders, 1982](#)), with a damping factor set to 10^{-2} . In this method, the elements of \mathbf{A} are applied as operators, so it is not necessary to build the referred matrix. The solution of Eq. 1 based on a least-squares scheme is referred to as LSMME, which does not require to satisfy a stability criterion, unlike the conventional MME scheme.

The conventional and causal imaging condition

The governing imaging condition for acoustic RTM is defined by the zero-lag cross-correlation of the source wavefield (P_S) with the receiver wavefield (P_R). This imaging condition is defined as follows

$$I_{cc}(\mathbf{x}) = \int_0^T P_S(\mathbf{x}, t) P_R(\mathbf{x}, t) dt \quad (8)$$

where $\mathbf{x} = (x, z)$ denotes the spatial coordinate, T is the maximum time recorded and I_{cc} is known as the conventional imaging condition. However, the application of Eq. 8 generally produces an image contaminated by strong RTM artifacts, which are generated by the undesired cross-correlation of head waves, diving waves,

and backscattered waves ([Yoon and Marfurt, 2006](#)).

An important approach that has been used to suppress RTM artifacts due to backscattered waves is to modify the imaging condition, which allows us to distinguish between the reflection and transmission images. In this way, [Revelo and Pestana \(2019\)](#) used a causal imaging condition that correlates the down-going component of the source, P_S^+ , with the up-going component of receiver wavefield, P_R^- , as proposed by [Shen and Albertin \(2015\)](#)

$$I_{causal}(\mathbf{x}) = \int_0^T P_S^+(\mathbf{x}, t) P_R^-(\mathbf{x}, t) dt, \quad (9)$$

where the + direction is defined away from the source. This imaging condition correlates wavefields only in points in space that correspond to seismic reflectors, generating the reflection image and avoiding RTM artifacts.

To obtain the individual components involved in Eq. 9, we use a via plane-wave-based decomposition scheme ([Shen and Albertin, 2015](#); [Revelo and Pestana, 2019](#)), for which it is necessary to introduce the analytical wavefield. The complex wavefield is defined as $\hat{P} = P(\mathbf{x}, t) + iQ(\mathbf{x}, t)$, where $Q(\mathbf{x}, t) = H\{P(\mathbf{x}, t)\}$ and $H\{\cdot\}$ is the Hilbert transform operator. For general media, this complex pressure wavefield \hat{P} satisfy a first-order partial equation in time ([Zhang and Zhang, 2009](#)). A conventional procedure to compute the analytical wavefield was proposed by [Shen and Albertin \(2015\)](#), but in their case the wave equation has to be solved twice, once for the source and another for the Hilbert transformed source. [Revelo and Pestana \(2019\)](#) presented an improved method to calculate the analytical wavefield stably and free of dispersion noise, using just a single propagation and based on the rapid expansion method (REM) ([Pestana and Stoffa, 2010](#)). Now, the source wavefield is extrapolated in time and for each time step the first-order time derivative is computed and then the Hilbert transform of the wavefield is obtained by applying the following relation between Q and P ([Zhang and Zhang, 2009](#))

$$Q(\mathbf{x}, t) = \frac{1}{L} \frac{\partial P(\mathbf{x}, t)}{\partial t}, \quad (10)$$

where L is a pseudo-differential operator in the space domain, defined by $L = v(\mathbf{x})\sqrt{-\nabla^2}$ and ∇^2 is Laplacian operator. Its symbolic representation is $L = v(\mathbf{x})\sqrt{k_x^2 + k_z^2}$ where k_x and k_z are the wavenumber components and $v(\mathbf{x})$ is the propagation velocity in the medium.

In the causal imaging condition the down-going component of source wavefield, P_S^+ , and the up-going component of receiver wavefield, P_R^- , are correlated to obtain the resulting imaging using Eq. 9. To obtain individual wavefield components involved in Eq. 9, following [Shen and Albertin \(2015\)](#), we use a Fourier transform in depth of the analytical wavefield considering mono frequency components ([Liu et al., 2011](#)). The down-going component of source wavefield, P_S^+ , in space and time, becomes

$$P_S^+(x, z, t) = \text{FFT}_z^{-1} \{ \kappa(k_z) \text{FFT}_z [\hat{P}_S(x, z, t)] \}, \quad (11)$$

where,

$$\kappa(k_z) = \begin{cases} 0 & \text{if } k_z \geq 0 \\ 1 & \text{if } k_z < 0 \end{cases} \quad (12)$$

and \hat{P}_S is the source analytical wavefield. The up-going receiver wavefield component in forward time, P_R^- , is obtained using the analytical receiver wavefield in Eq. 11 and replacing κ by $1 - \kappa$ in Eq. 12. In this paper, we apply a Hann window on Eq. 12 to smooth the filter, so the vertical stripes over the entire panel due to the FFT of discontinuous functions are attenuated.

In summary, in our implementation, we are proposing to use the LSMME scheme to retrieve the dataset free of internal multiple reflections. After that, the LSMME output dataset is migrated, using RTM, and the causal imaging condition is applied based on the method proposed by Revelo and Pestana (2019). Thus, combining both techniques, we can effectively suppress the undesired RTM artifacts, which are typically present in the conventional RTM results.

NUMERICAL EXAMPLE

In the following, we use a 2D synthetic model to illustrate the benefits of the procedure proposed in this work. The acoustic velocity model is composed of flat layers and a reservoir zone (Figure 1). The model consists of 1751×2627 grid nodes with 2m grid spacing. The synthetic acoustic impulse reflection responses, for a fixed-spread geometry, are generated with a finite-difference time-domain modeling code (Thorbecke and Draganov, 2011), and the input source signature is approximately a *sinc* function with a flat spectrum of unitary amplitude. We apply absorbing boundaries on all sides, i.e., we assume that surface-related multiples and ghost wave effects are removed from the recorded dataset. The direct wave in the recorded data was removed by modeling it separately in a homogeneous medium (values of the first layer) and then subtracting it from the recorded data. We simulated the single-sided reflection responses with 526 sources and a fixed-spread geometry that ranges from -2626 to 2626 m with a 10m distance between sources and also between receivers, which are located at the top of the model. The duration of each shot record is 3.204s sampled at 4ms. It is important to note that the operators \mathbf{R} and \mathbf{R}^* are applied by using the impulse reflection responses. For the application of the LSMME scheme and the RTM algorithm, the synthetic acoustic reflection responses are obtained from the convolution of R with a Ricker source wavelet with a central frequency of 20Hz.

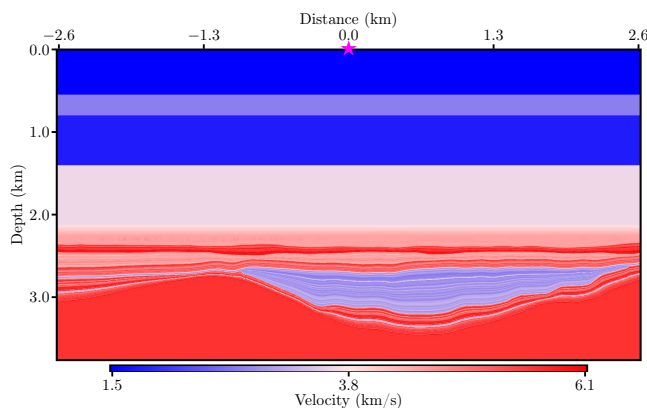


Figure 1: Velocity model.

Figure 2a shows the central shot (purple star in Figure

1), where we can see the presence of internal multiple reflections that were marked by the red arrows. We use the computed single-sided impulse reflection responses as input to solve Eqs. 1 and 2 through the LSMME scheme. The number of iterations for the LSMME technique is set at 20. Figure 2b shows the retrieved reflection response without internal multiples using the aforementioned method for the central shot gather. This result clearly shows that the most of internal multiple reflections in Figure 2a were attenuated as a result of the application of the LSMME. The orange and blue dashed lines in Figure 2a-b represent the zero-offset trace positions that were selected for a more detailed analysis. In Figure 2c we perform a comparison between these traces, and we can see that the LSMME scheme correctly eliminates the events associated with internal multiple reflections and that the primary reflections coincide well, thus preserving their amplitude and phase. A similar result was also presented in Santos et al. (2020a), where it is shown that the LSMME scheme is capable of maintaining the characteristics of the primary events, attenuating only the multiple noises.

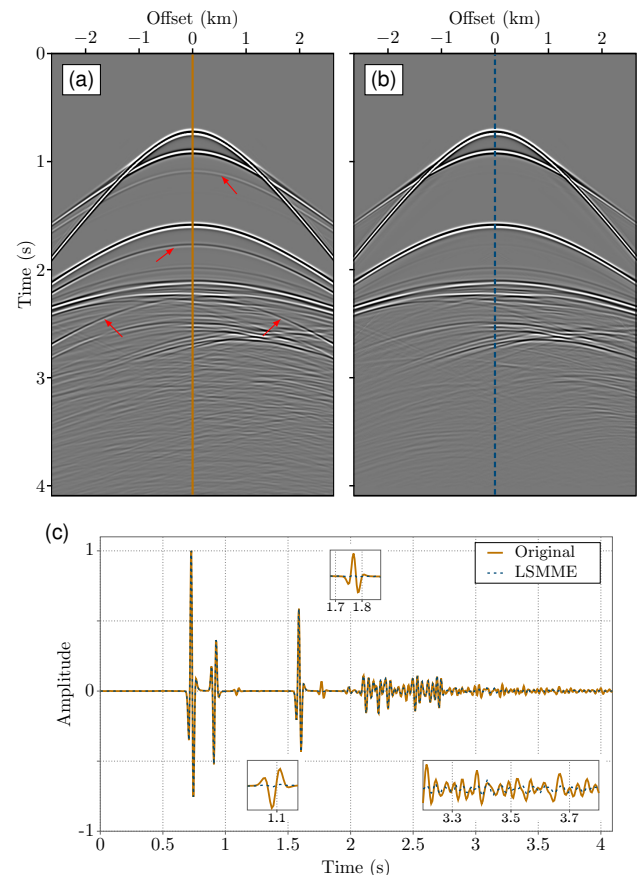


Figure 2: (a) The modeled reflection response and (b) the retrieved reflection response using the LSMME scheme. (c) The comparison of zero-offset traces.

Continuing with our analysis, a synthetic modeling is presented to validate the method to construct the analytical wavefield and apply the causal imaging condition. Figure 3a shows the pressure snapshot at 1.4s of an acoustic wavefield due to a 20Hz-peak-frequency Ricker-wavelet source located at the origin of the coordinate system (purple star in Figure 1) with a time sampling of 4ms. Figure

3b shows the imaginary part, Q , of the analytical wavefield obtained by using a single wave-equation solution, through the REM method. We take as input the analytical wavefield (Figure 3a-b) and perform the explicit wavefield separation using Eqs. 11 and 12. A 20-point Hann window is also applied to remove vertical stripes artifacts. Figures 3c and 3d show the up-going component (reflected waves) and the down-going component (transmitted waves), respectively. With these results, we demonstrate that the analytical wavefield, as well as the unidirectional components of the acoustic wavefield are constructed, and therefore can be used in the application of causal RTM.

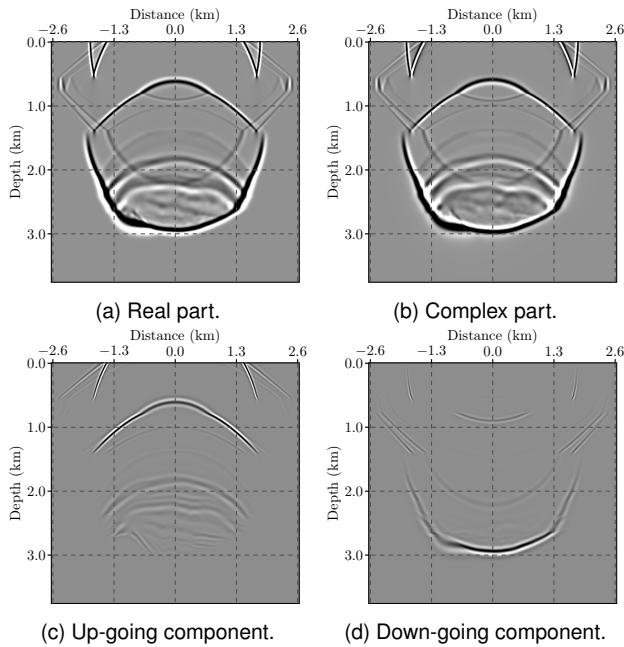


Figure 3: Snapshots for source wavefield at $t = 1.4$ s for the real and complex parts and for the up- and down-going wavefields.

In the following, we apply the RTM without and with up-down wavefield decomposition using as input the original reflection responses and the retrieved dataset by the LSMME scheme. A comparison between the migrated images is shown in Figure 4. In the conventional migration results, dominant low-wavenumber artifacts are generated, which are introduced by the cross-correlation of the back-scattered fields. Figure 4a-b shows the RTM results obtained by conventional correlation imaging condition followed by application of the Laplacian filter and also the RTM results using the causal imaging condition (Figures 4c and 4d). The image in Figure 4a contains artifacts (indicated by the red arrows and ellipse) from internal multiple reflections because they are imaged as if they were primary reflections. Furthermore, it is observed that the reflected interbeds are artificially imaged by the conventional imaging condition (marked by the blue arrows and rectangle), mainly on top of the fourth reflector. However, the image in Figure 4b, which are obtained from the retrieved dataset, are free of artifacts caused by the internal multiples, but still with the presence of the false reflectors built in the conventional RTM.

Figures 4c and 4d are results obtained applying the causal imaging condition, where the input data for the RTM

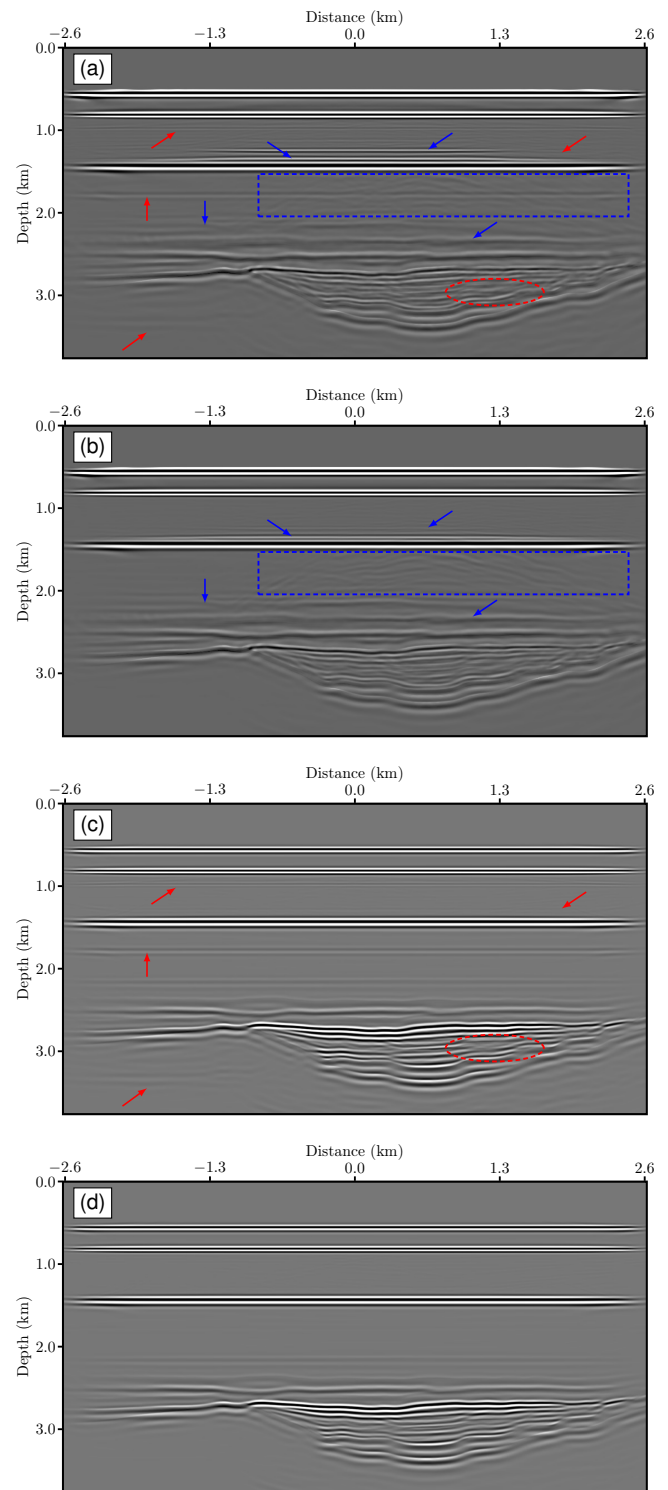


Figure 4: RTM results images, (a)-(c), using the modeled reflection responses and (b)-(d) the recovered primary reflections by the LSMME scheme. (a) and (b) are images obtained by applying the conventional cross-correlation and (c) and (d) by the causal imaging condition.

algorithm was the original dataset and the internal multiple-free reflection responses, respectively. We should notice that these results have a better quality compared to Figures 4a and 4b and that the artifacts above the fourth interface, as well as those indicated by the blue arrows, are

removed by directionally decomposing wavefields before imaging. Comparing the causal RTM results, in Figure 4d we no longer have the artifacts related to the internal multiple reflections. These results confirm the successful application of RTM when using LSMME filtering, combined with the computation of the analytical wavefield which allows us to separate the wavefield for application of the causal imaging condition shows the effectiveness of the implemented algorithm for removing artifacts (Figure 4d) usually seen in a typical RTM (Figure 4a).

CONCLUSIONS

Reverse-time migration can produce accurate images of the subsurface. However, the resulting image can be contaminated by artifacts related to the internal multiple reflections or to the conventional correlation-based imaging condition. Therefore, the data resulting from high-quality processing and a correct imaging condition must be applied to remove artifacts from RTM images. In this paper, we have presented a procedure that combines two efficient schemes to improve the migrated sections. In the data domain, we implemented the LSMME scheme to filter the multiple internal reflections. The RTM result, using as input the retrieved dataset, shown that the application of this method contributes to generating a better image, free of ghost reflectors caused by the internal multiples. Furthermore, in the model domain, we implemented and demonstrated that the causal imaging condition can effectively remove the undesired artifacts and low-frequency noise produced by the cross-correlation imaging condition. We then performed causal RTM on the LSMME dataset. From this migrated image, we demonstrated that the application of both schemes has produced high-quality results when compared with the conventional RTM of the original dataset.

ACKNOWLEDGMENTS

This work was supported by CENPES/Petrobras through the Marchenko project at SENAI-CIMATEC. The authors also wish to thank to the developer team of the Open-Source libraries in TUDelft. A special acknowledgment to the geophysical team at SENAI-CIMATEC for discussions and contributions.

References

- Baysal, E., D. D. Kosloff, and J. W. Sherwood, 1983, Reverse-time migration: *Geophysics*, **48**, 1514–1524.
- , 1984, A two-way nonreflecting wave equation: *Geophysics*, **49**, 132–141.
- Fletcher, R., P. Fowler, P. Kitchenside, and U. Albertin, 2006, Suppressing unwanted internal reflections in prestack reverse-time migration: *Geophysics*, **71**, E79–E82.
- Guitton, A., B. Kaelin, and B. Biondi, 2007, Least-squares attenuation of reverse-time migration artifacts: *Geophysics*, **72**, S19–S23.
- Hu, L. and G. A. McMechan, 1987, Wave-field transformations of vertical seismic profiles: *Geophysics*, **52**, 307–321.
- Liu, F., G. Zhang, S. Morton, and J. Leveille, 2011, An effective imaging condition for reverse-time migration using wavefield decomposition: *Geophysics*, **76**, S29–S39.
- McMechan, G. A., 1983, Migration by extrapolation of time-dependent boundary values: *Geophysical Prospecting*, **31**, 413–420.
- Paige, C. and M. Saunders, 1982, Algorithm 583. LSQR: Sparse linear equations and least squares problems: *ACM Transactions on Mathematical Software*, **8**, 195–209.
- Pestana, R. C. and P. L. Stoffa, 2010, Time evolution of wave equation using rapid expansion method: *Geophysics*, **75**, T121–T131.
- Revelo, D. E. and R. C. Pestana, 2019, Up/Down acoustic wavefield decomposition using a single propagation and its application in reverse time migration: *Geophysics*, **84**, no. 4, S341–S353.
- Santos, R. S., D. E. Revelo, R. C. Pestana, V. Koehne, D. F. Barrera, and M. S. Souza, 2020a, A least-squares based approach for the Marchenko internal multiple elimination scheme, in *SEG Technical Program Expanded Abstracts 2020*, 3184–3188, Society of Exploration Geophysicists.
- Santos, R. S., M. S. Souza, D. F. Barrera, D. E. Revelo, and V. Koehne, 2020b, Fast Marchenko multiples elimination on CMP processing, in *SEG Technical Program Expanded Abstracts 2020*, 3189–3193, Society of Exploration Geophysicists.
- Shen, P. and U. Albertin, 2015, Up-Down separation using Hilbert transformed source for causal imaging condition, in *SEG Technical Program Expanded Abstracts 2015*, 4175–4179, Society of Exploration Geophysicists.
- Thorbecke, J. and D. Draganov, 2011, Finite-difference modeling experiments for seismic interferometry: *Geophysics*, **76**, no. 6, H1–H18.
- van der Neut, J. and K. Wapenaar, 2016, Adaptive overburden elimination with the multidimensional Marchenko equation: *Geophysics*, **81**, no. 5, T265–T284.
- Yoon, K. and K. J. Marfurt, 2006, Reverse-time migration using the Poynting vector: *Exploration Geophysics*, **37**, 102–107.
- Zhang, L. and E. Slob, 2019a, A field data example of Marchenko multiple elimination: *Geophysics*, **85**, 1–39.
- , 2019b, Free-surface and internal multiple elimination in one step without adaptive subtraction: *Geophysics*, **84**, A7–A11.
- , 2020a, A fast algorithm for multiple elimination and transmission compensation in primary reflections: *Geophysical Journal International*, **221**, 371–377.
- , 2020b, Marchenko multiple elimination of a laboratory example: *Geophysical Journal International*, **221**, 1138–1144.
- Zhang, L. and M. Staring, 2018, Marchenko scheme based internal multiple reflection elimination in acoustic wavefield: *Journal of Applied Geophysics*, **159**, 429–433.
- Zhang, L., J. Thorbecke, K. Wapenaar, and E. Slob, 2019, Transmission compensated primary reflection retrieval in the data domain and consequences for imaging: *Geophysics*, **84**, Q27–Q36.
- Zhang, Y. and J. Sun, 2009, Practical issues in reverse time migration: True amplitudes gathers, noise removal and harmonic-source encoding: *First Break*, **26**, 19–25.
- Zhang, Y. and G. Zhang, 2009, One-step extrapolation method for reverse time migration: *Geophysics*, **74**, no. 4, A29–A33.